Original Research

IP3R-1 aggravates endotoxin-induced acute lung injury in mice by regulating MAM formation and mitochondrial function

Shuan Dong*, Ya Wu*, Yuan Zhang*, Shaona Li, Qin Zhao, Shasha Liu, Yan Guo, Xiangyun Li, Kai Song, Lili Wu, Lina Wu, Jia Shi, Lirong Gong and Jianbo Yu

Department of Anesthesiology and Critical Care Medicine, Tianjin Nankai Hospital, Tianjin Medical University, Tianjin 300100, China
*These authors contributed equally to this paper.
Corresponding author: Jianbo Yu. Email: 30717008@nankai.edu.cn

Impact Statement

Acute lung injury (ALI) caused by sepsis is the critical clinical illness, whose mortality rate is still as high as 40%. Organelle dysfunction has become a hot topic in the study of sepsis-induced ALI pathogenesis. In the study, we demonstrated increased mitochondria-associated endoplasmic reticulum membrane (MAM) formation, significant morphological changes in the mitochondria, and increased type-1 inositol-1,4,5-trisphosphate receptor (IP3R-1) expression in lung tissues of mice using the endotoxin-induced ALI model. MAM formation was reduced, and mitochondrial function was partially normalized when IP3R-1 function was silenced. Therefore, IP3R-1 plays an indispensable role in MAM formation and mitochondrial dysfunction, which could be innovative therapeutic targets for endotoxin-induced ALI.

Abstract

Acute lung injury (ALI) caused by endotoxin represents one of the common clinical emergencies. Mitochondria-associated endoplasmic reticulum membranes (MAM) serve as a critical link between mitochondria and endoplasmic reticulum (ER), which has an essential effect on maintaining intracellular homeostasis. As an important component of MAM, type-1 inositol-1,4,5-trisphosphate receptor (IP3R-1) mediates the ER-to-mitochondrial transport of Ca^{2+}. This study explored the role of IP3R-1 and MAM in ALI. Besides the levels of inflammasome-associated components interleukin (IL)-6, tumor necrosis factor (TNF)-α, and malonyldialdehyde (MDA) were increased in both bronchoalveolar lavage fluid (BALF) and serum, increased cross-sectional area of mitochondria, elevated MAM formation, and decreased respiratory control ratio (RCR) were observed within lung tissues collected in lipopolysaccharide (LPS)-treated mice, accompanied by upregulation of IP3R-1 in total lung lysates and MAM. Ca^{2+} uptake level in the mitochondria, production of reactive oxygen species (ROS) in the mitochondria, and the formation of MAM were elevated within LPS-treated MLE-12 cells, and all those changes in response to LPS were partly inhibited by knocking down of IP3R-1 expression in MLE-12 cells. Collectively, IP3R-1 has a critical effect on MAM formation and mitochondrial dysfunction, which could be innovative therapeutic targets for ALI caused by endotoxin.

Keywords: Endotoxin-induced acute lung injury, MAM, IP3R-1, mitochondria, Ca^{2+}

***Experimental Biology and Medicine* 2023; 248: 2262–2272. DOI: 10.1177/15353702231220667**

Introduction

Sepsis refers to the impaired infection immune response of the host that leads to the severe organ dysfunction.[1] Nearly 45% of sepsis patients develop multiple organ dysfunction, and it has become one of the main burdens of public health worldwide.[2,3] The lung represents a vulnerable organ, which gets affected in nearly 40% of sepsis patients, and sepsis-induced ARDS induces results in a high mortality rate related to severe sepsis or septic shock.[4]

Although the exact molecular mechanism is poorly determined, cell organelle dysfunction, like mitochondria and endoplasmic reticulum (ER), is an important process in pathogenesis of sepsis-induced acute lung injury.[5,6] Markers of ER stress, including GRP78 and CHOP, were increased markedly in lung tissues from lipopolysaccharide (LPS)-mediated mice, and ER stress-alleviating interventions can reduce pro-inflammatory protein expression.[7] It has also been established in mouse models and human studies that endotoxin-induced acute lung injury results in mitochondrial dysfunction, including a decline in oxidative capacity, ultrastructure abnormalities, increased oxidative stress, and altered dynamic balance.[8] MAM belongs to the subdomain of ER, which is the physical contact between mitochondria and ER.[9] MAM is the signal communication platform and has a crucial effect on multiple cell activities, such as lipid metabolism, Ca^{2+} homeostasis, autophagy, or regulating apoptosis.[10–12]

There are many articles identifying the impact of MAM on Ca^{2+} homeostasis in recent years. Mitochondria fulfill various key roles in cellular metabolism, and mitochondrial Ca^{2+} level has an important role in maintaining mitochondrial

bioenergetics, such as adenosine triphosphate (ATP) synthesis and tricarboxylic acid (TCA) cycle.[10–12] MAM is comprised by ER subdomain, specific proteins that are enriched preferentially at the MAM, and outer mitochondrial membrane. MAM facilitates intracellular Ca^{2+} transport between mitochondria and ER,[13] regulating Ca^{2+} concentration in mitochondria or other mitochondrial functions.[14,15] It was indicated that enhanced MAM generation promotes mitochondrial calcium accumulation, thus causing impaired oxidative ability of mitochondria, enhanced reactive oxygen species (ROS) production and cellular stress.[16] Furthermore, downregulating critical factors related to calcium flux (like IP3R-1) and ER-mitochondria contract could reduce cellular stress, promote mitochondrial respiration, while enhancing glucose tolerance of obese animals.[16]

Recently, more evidence indicated that disruption of MAM integrity is regarded as a cornerstone in disease pathogenesis, like type 2 diabetes mellitus (T2DM), amyotrophic lateral sclerosis/frontotemporal dementia (ALS/FTD), Alzheimer's disease (AD), Parkinson's disease (PD), cancer and cardiovascular diseases (CVD),[17–19] but the relevance of structural integrity of the MAM in endotoxin-induced ALI remains to be further studied; therefore, this work is conducted to gain more insight into this important issue.

Materials and methods

Experimental animals

Every animal protocol gained approval from Animal Ethical and Welfare Committee (AEWC) of Tianjin Nankai Hospital (NKYY-DWLL-2019–027). Male C57BL/6 mice (6- to 8-week-old) with body weights ranging from 20 to 24 g were used in our study (Division of Animal Resources at Tianjin Nankai Hospital, Tianjin). Mice were later randomized as endotoxin-treated (LPS) and normal saline (control) groups. All the animals were maintained at the Division of Animal Resources at Tianjin Nankai Hospital. Mice were housed in ventilated cages (maximum of five per cage) and maintained at 12-h light and dark cycles.

LPS administration and experimental protocols for animals

Each mouse was injected with either normal saline (NS) or a non-lethal dose (15 mg/kg) of LPS (O111:B4, Sigma) into the tail vein to establish the endotoxin-induced ALI mouse model *in vivo*. After 12 h of injections, mice were euthanized, and then lung tissue was dissected in subsequent experiments. We also obtained blood and bronchoalveolar lavage fluid (BALF) samples in all animals before euthanization and used for the quantification of pro-inflammatory cytokines and oxidative stress markers.

Cell culture

MLE-12, a murine lung epithelial cell line, was cultured and maintained in a T25 culture bottle (Corning, 430168) in Dulbecco's Modified Eagle's Medium (DMEM) (Hyclone, SH30023.01) supplemented with 2% heat-inactivated fetal calf serum (Excellbio, FSP500), ITS liquid media supplement (Sigma, I1884), β-estradiol (Sigma, E2758), hydrocortisone (Sinopharm, 66003632), HEPES (Shanghai basal media, B110), and L-glutamine (Sigma, G8540) under 37°C and 5% CO_2 conditions. Cells (5×10^4/well) were later inoculated into the 96-well plate (Sigma, SIAL0596), maintained in DMEM overnight, and then washed with PBS twice prior to experimentation.

LPS attacking cell models and cell counting kit-8

The LPS of *Escherichia coli* (O111:B4, L2630, Sigma-Aldrich, St. Louis, MO, USA) was used for inflammation induction. In brief, LPS (40 μg/mL) was added for 24 h cell treatment. Cell counting kit (CCK)-8 (EnoGene, Nanjing, China) was used to assess the cell viability. Briefly, after LPS stimulation, medium was introduced with 10 μL CCK-8 reagent, for 2 h culture under 37°C. A microplate reader (Rayto RT-6000, Shenzhen, China) was utilized to detect absorbance at 450 nm.

Cell transfection

GenePharma Co. (Shanghai, China) was responsible for synthesizing IP3R-1-targeted siRNA together with corresponding negative controls (NC-siRNA). Afterwards, Lipofectamine 3000 reagent (Invitrogen, Waltham, MA, USA) was utilized for cell transfection in line with specific instructions.

Determination of the wet-dry ratio

After euthanasia of mice, lung tissue was separated and put into the tared microcentrifuge tube, followed by measurement of wet weight. Thereafter, lung tissue was put into a desiccator for a 24-h period under 55°C for obtaining dry weight. Afterwards, wet-dry ratio (a reflection of pulmonary edema) was obtained through dividing wet by dry lung mass.

Pro-inflammatory cytokine and malonyldialdehyde levels as well as superoxide dismutase activity within BALF and serum

Interleukin (IL)-6, tumor necrosis factor (TNF)-α, and malonyldialdehyde (MDA) levels together with superoxide dismutase (SOD) activity within BALF and serum were detected by the commercial kits (R&D Systems, Minneapolis, MN, USA) in line with specific instructions.

Isolation and identification of MAM from the lungs

The subcellular fractionation of the lung lysates was carried out by differential centrifugation with minor modifications based on published protocols,[20] as shown in Supplementary Figure 1. MAM was identified by the expression of characteristic proteins, as can be seen in Supplementary Figure 2. IP3R-1 was mainly found in the ER fractions, Cyto C was enriched in mitochondrial fractions, calnexin and protein disulfide-isomerase (PDI) showed equal distribution between MAM and ER, while Sig-1R was preferentially located at the MAM.

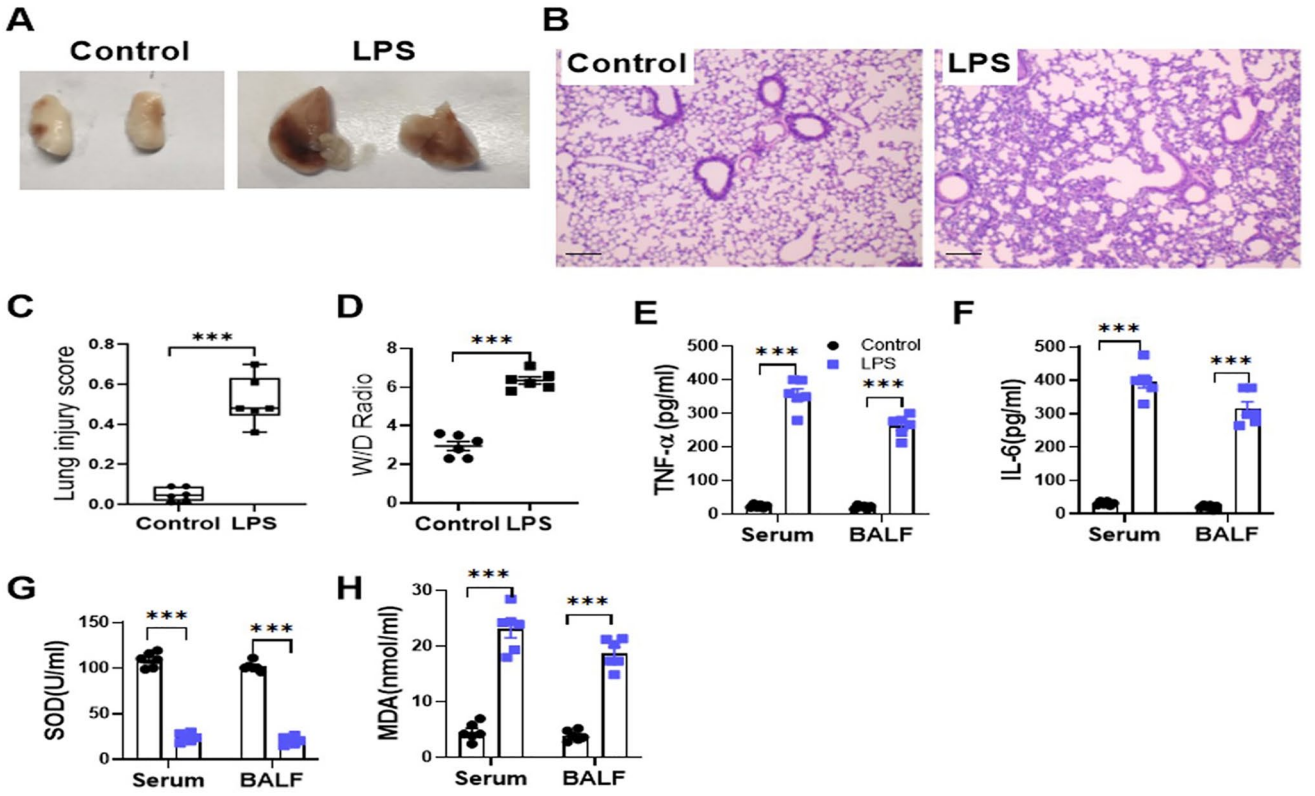

Figure 1. Administration of endotoxin could lead to severe lung injury. Data are presented for the lungs harvested from LPS-treated and control mice. (A) The gross morphology of the isolated lungs. (B) The photomicrographs showing sections under H&E staining. Scale bar = 100 μm. (C) Lung injury score assessment. (D) Lung wet/dry weight ratio. (E) to (H) ELISA for TNF-α, IL-6, and MDA-7 protein expression (E to G) and SOD activity (H) in the serum and BALF. The ALI scores were represented as median (Min, Max) and analyzed by Mann–Whitney *U*-test. $n = 6$; ***$P < 0.001$. In (E) to (H), all bars indicate mean ± SEM. $n = 6$; ***$P < 0.001$; Student's *t*-test.

Histopathology

After perfusion using 4% paraformaldehyde, lung tissue was processed through paraffin embedding, sectioning along with hematoxylin and eosin (H&E) staining. Stained slides were examined under a microscope to determine the morphology and inflammatory infiltrates in the lung sections. The evaluation of lung injury was performed in line with the official report delivered by the American Thoracic Society in 2011.[21] Then, this work scored 20 randomly non-overlapping fields under high-power fields (×400) from per animals independently. Alveolar septal thickness, hyaline membranes, proteinaceous debris, neutrophil number within interstitial space, and alveolar space were assessed by two experienced pathologists blinded to study nature. Each pathologic characteristic was weighted according to the relevance and determined based on the assessed field number.

Transmission electron microscopy

Lung samples with a volume of less than 1 cubic centimeter were selected for transmission electron microscopy (TEM) evaluation. Fixation and sectioning of the lung tissues were carried out as described previously. Ultrathin sections were examined under a Tecnai microscope. Lung sections taken from the same lobe of the control and LPS groups were examined, and images of each group were captured at 5000× and 11,500× magnifications. Image J application (National Institutes of Health, USA) was employed for image analysis. Total number and the cross-sectional area of the mitochondria per field were calculated. To quantify MAM level, mitochondria linked with the ER was normalized to the total mitochondria perimeter. Two independent investigators blind to the treatments quantified the images.

Extraction of total protein and western blotting

After homogenization of lung tissues (50 mg) in cold lysis buffer, the homogenate was subjected to 10 min centrifugation at 9000 r/min for pelleting cell debris. Thereafter, supernatants were harvested to estimate protein concentration by the bicinchoninic acid (BCA) method. Later, 40 μg protein aliquots were separated by sodium dodecyl sulfate–polyacrylamide gel electrophoresis (SDS-PAGE) prior to transfer on polyvinylidene (PVDF) membranes as previously described.[22] Membranes were incubated with antibodies against type-1 inositol-1,4,5-trisphosphate receptor (IP3R-1) (1:1000, PTG, 19962, Wuhan, China), IP3R-2 (1:1000, Santa Cruz, 398434, USA), Mitofusin-2 (1:1000, PTG, 12186, Wuhan, China), sigma-1 receptor (Sig-1R) (1:1000, PTG, 15168, Wuhan, China), PDI (1:1000, Cell Signaling, 2446, USA), PACS-2 (1:1000, PTG, 19508, Wuhan, China) and beta-actin (1:8000, Tianjin Sungene Biotech Co., KM9001, Tianjin, China) under 4°C over-night, followed by incubation using a horseradish perox-idase–labeled secondary antibody (1:10000, Amersham Biosciences, GBR). Then, the integrated optical density (IOD) of each protein was determined

using Quantity One 4.62 (Bio-Rad, Hercules, CA, USA). The validation of the IP3R-1 antibody was determined by the siRNA-mediated knockdown of IP3R-1. We cut membranes prior to blotting, so that there was no full-length blot. Supplementary Files displays uncropped images.

Mitochondrial respiratory activity

Mitochondrial isolation and purification were completed in line with aforementioned description. Later, oxygen consumption in the separated mitochondria was monitored with GENMED mitochondria respiratory control ratio (RCR) kits (GENMED, Shanghai, China) by the Clark-type oxygen electrode (Hansatech, UK) to assess mitochondrial respiratory activity. The protocols were following the instruction of the manufacturer. Finally, 10 µL Reagent B (state 4 [ST4]) and 10 µL Reagent C (state 3 [ST3]) were added to terminate reaction. We calculate and report the RCR by dividing state 3 by state 4.

Flow cytometry

Lung tissues were digested, and cells were collected. The probe for MitoSOX (ThermoFisher (Waltham, MA, USA), M36008), TMRM (ThermoFisher, I34361), or Rhod-2 AM (ThermoFisher, R1245MP) was added to the cell suspension as recommended in the manual. The cell suspension was then analyzed by CytoFLEX S (Beckman Coulter, Brea, CA, USA), and WinMDI 2.9 was employed for data analysis, which were expressed as mean fluorescence intensity (MFI).

Visualization of voltage-dependent anion channel/IP3R-1 complex by immunofluorescence

After fixation within 4% PBS, cells were subjected to permeabilization using 0.3% Triton X-100. Thereafter, cells were blocked using 2% bovine serum albumin (BSA) contained within PBS prior to overnight incubation using primary antibodies against voltage-dependent anion channel (VDAC)-1 (Abcam, ab14734) and IP3R-1 (Abcam (Cambridge, UK), ab264281). After three washes, Alexa Fluor secondary antibodies (Abcam, ab150077, ab150080) were added for further cell incubation. The nuclei were stained with 4′,6-diamidino-2-phenylindole (DAPI) (Abcam, ab228549) and mounted with fluorescent mounting media. The Nikon Eclipse Ti-U fluorescence microscope (Nikon Corp., Tokyo, Japan) was adopted for image capturing. VDAC-1 was stained with DsRED, IPR3-1 was stained with fluorescein isothiocyanate (FITC), and the nucleus was stained with DAPI. Colocalization of VDAC-1 and IP3R-1 appeared as yellow color. The colocalization between VDAC-1 and IP3R-1 expressions was analyzed using the "Colocalization Threshold" module in Fiji/Image J.

Statistics

ALI scores were expressed as median (Min, Max) and analyzed by one-tailed Mann–Whitney *U*-test, other data were represented by mean ± SEM. Unpaired Student's *t*-test (two-tailed) or one-way analysis of variance (ANOVA) of repeated experiments plus Tukey's post hoc pairwise multiple comparisons was adopted to compare two groups using Prism 8 (GraphPad). $P < 0.05$ stood for statistical significance.

Results

Endotoxin-induced lung injury caused enhanced ER–mitochondria interaction in the lung

Gross morphology of isolated lungs was examined 12 h after administration of either endotoxin or saline. Endotoxin-treated lungs appeared swollen and congested in comparison with control group (Figure 1(A)). LPS treatment led to a higher lung injury score compared to control treatment (Figure 1(B) and (C)). Lung wet/dry (W/D) ratio of LPS-treated mice markedly increased (Figure 1(D)). TNF-α, IL-6, and MDA levels also increased within BALF and serum of LPS-treated mice, but the SOD activity decreased significantly in LPS-treated mice (Figure 1(E) to (H)).

In order to investigate the ER–mitochondria interaction using an LPS-induced ALI model, lung sections collected from both the control and LPS groups were examined by TEM. Lungs from the LPS-treated mice displayed morphological changes in the mitochondria, including swelling, vacuole formation, and crest reduction. For LPS-mediated mice, their lung tissues showed the evidently elevated ER apposition to mitochondria (Figure 2(A)). The number of mitochondria per field marked decreased in LPS-treated lungs (Figure 2(B)); however, the cross-sectional area of the mitochondria significantly enlarged in the LPS-treated lungs due to the swollen mitochondrial morphology (Figure 2(C)). In addition, mitochondrial membrane-adjacent ER contact percentage of LPS-treated lungs apparently increased relative to controls (Figure 2(D)).

Next, we sought to determine whether the increased ER–mitochondrial interaction resulted in the altered oxidative capacity of mitochondria. We found that LPS administration decreased mitochondria ST3 oxygen consumption (Figure 2(E)) but increased ST4 oxygen consumption (Figure 2(E)), leading to the reduction of RCR levels far below the normal level of 3~10 (Figure 2(E)). Taken together, our results indicated that endotoxin-induced lung injury was associated with morphological alterations of the mitochondria, enhanced MAM formation, and impaired oxygen consumption in the mitochondria.

Endotoxin-mediated ALI resulted in upregulation of the proteins involved in ER to mitochondria calcium transport

To investigate the potential results of enhanced ER–mitochondrial interactions using the endotoxin-induced ALI model, this work analyzed MAM-associated protein levels within total lung lysates (Figure 3(A)). Our data demonstrated increased IP3R-1 protein expression and reduced mitofusin-2 protein level within total lung lysates of the LPS-treated mice than the control mice (Figure 3(B) and (D)). IP3R-2, PACS-2, and Sig-1R proteins were not significantly different in the total lung lysates between LPS-treated mice and control mice (Figure 3(C), (E) and (F)).

To elucidate the protein composition of crude mitochondria (CM), pure mitochondria (PM), ER, and MAM in the LPS-treated and control lung tissues, we first isolated subcellular fractions by Percoll-based density gradient centrifugation according to description in materials

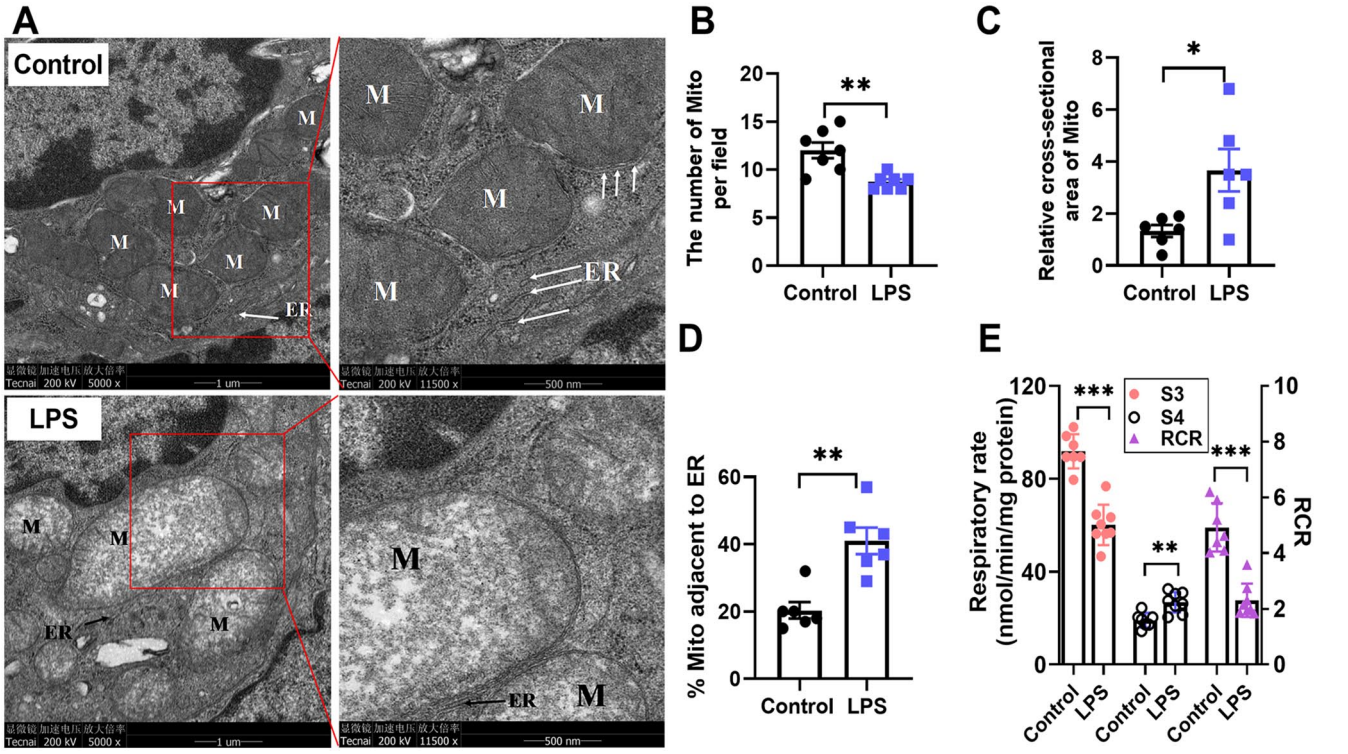

Figure 2. Endotoxin-induced lung injury leads to increased ER and mitochondrial interaction in the lung. Data are presented for the lungs harvested from LPS-treated and control mice. (A) Typical TEM images showing mouse lung sections after either endotoxin or saline challenge. Scale bar: 1 μm (right panel) and 500 nm (left panel). M: mitochondria (white arrow), ER: endoplasmic reticulum (black arrow). (B) to (D) The total number of mitochondria per field (B), the cross-sectional area of mitochondria per field (C), and the ratio between the percent of mitochondria connected to ER to the total mitochondrial perimeter (D). (E) Respiratory control ratio (RCR). All bars indicate mean ± SEM. $n = 6$~7; $^{*}P < 0.05$; $^{**}P < 0.01$; $^{***}P < 0.001$; Student's *t*-test.

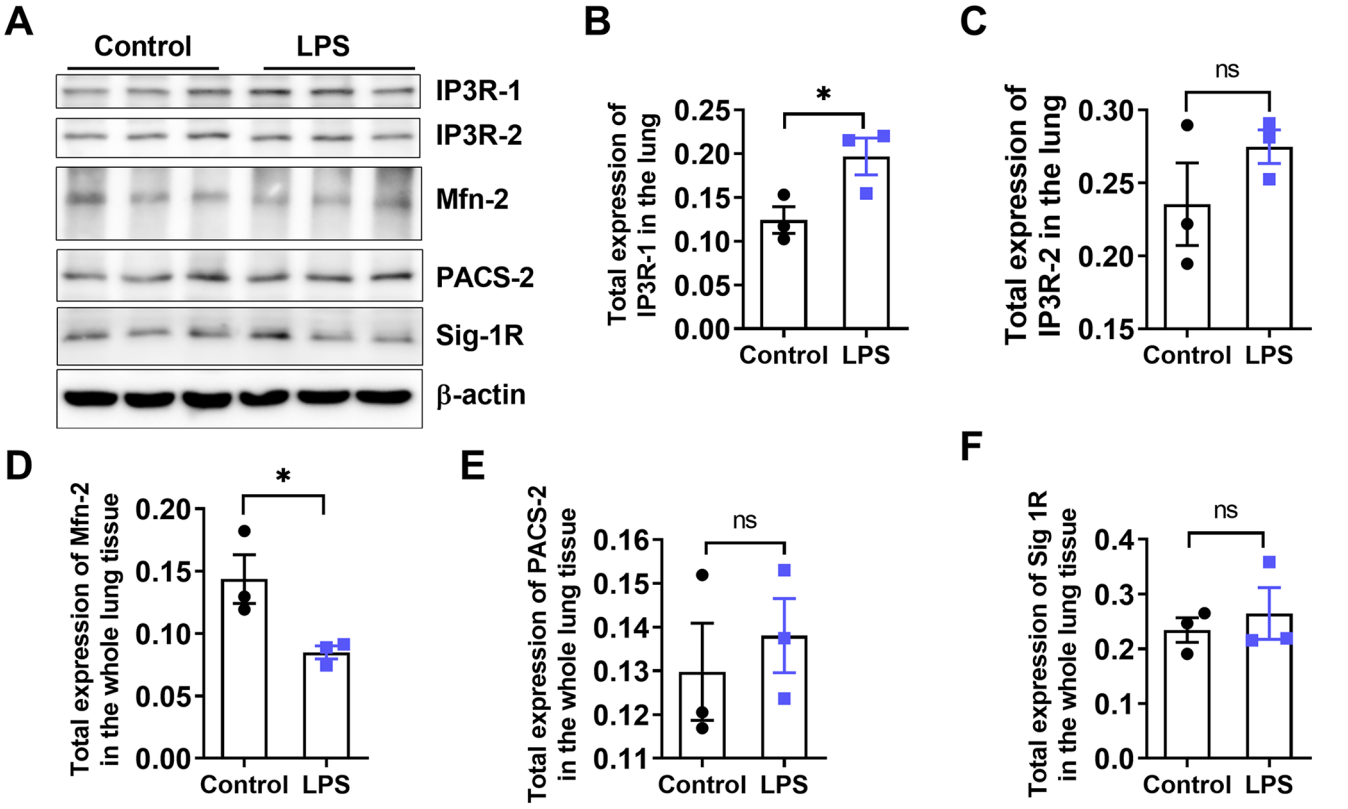

Figure 3. MAM-related protein expression in the total lung lysates collected in endotoxin-induced ALI mice. Data are presented for the lungs harvested from LPS-treated and control mice. (A) Western-blotting assay on the expression of IP3R-1, IP3R-2, Mfn-2, PACS-2, and Sig-1R protein levels within total lung lysates. (B) to (F) Protein quantification within the total lung lysates. All bars represent mean ± SEM. $n = 3$; $^{*}P < 0.05$; Student's *t*-test.

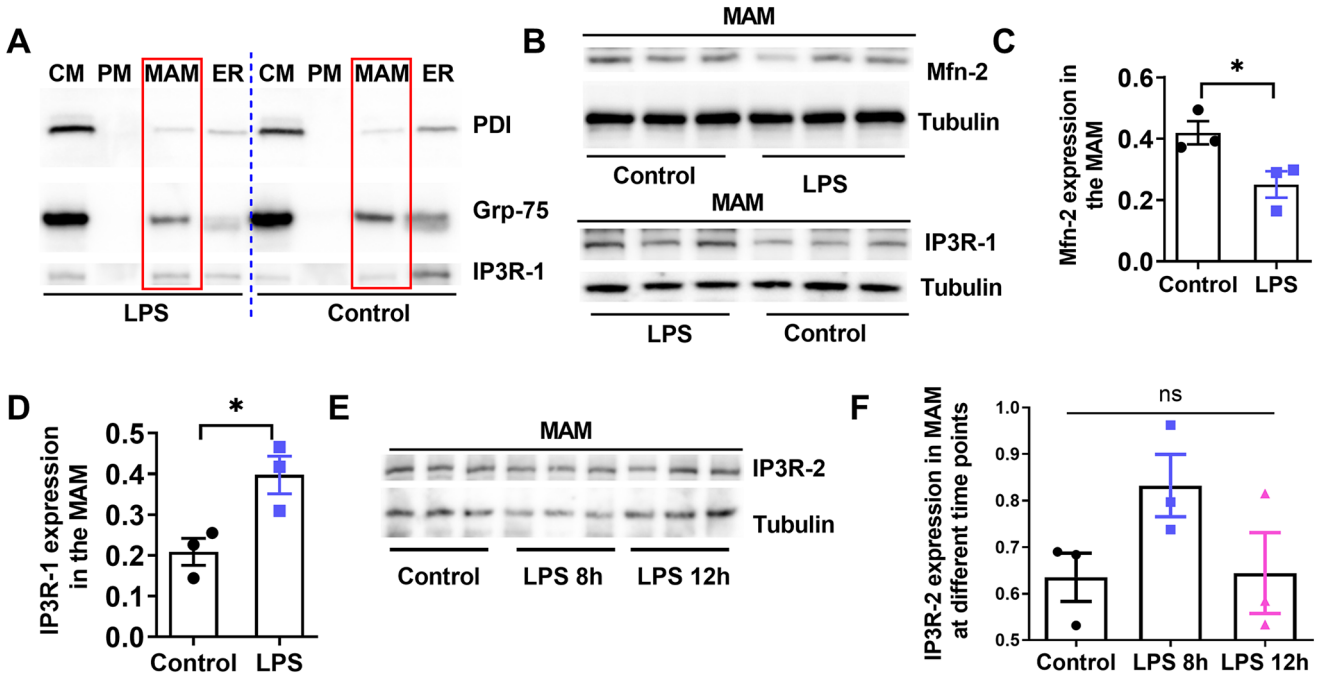

Figure 4. Western-blotting assay on the indicated proteins in different subcellular fractions of the lung lysates. Data are presented for the lungs harvested from LPS-treated and control mice. (A) Expression of PDI, Grp-75, and IP3R-1 from different subcellular fractions. (B) to (D) Expressions of IP3R-1 and Mfn-2 in the MAM fraction of the lung lysates. (E) and (F) Western-blotting assay and quantitative analysis on IP3R-2 expression kinetics in the MAM fractions. PM: pure mitochondria; CM: crude mitochondria; MAM: mitochondria-associated endoplasmic reticulum membranes; ER: endoplasmic reticulum. All bars indicate mean ± SEM. $^*P < 0.05$; $n = 3$; Student's *t*-test or one-way ANOVA.

and methods. We found that IP3R-1 expression apparently elevated, whereas mitofusin-2 expression dramatically declined within the MAM fractions of the lung lysates among LPS-mediated mice relative to control mice (Figure 4(A) to (D)). To determine the kinetics of IP3R-2 expression, we collected the MAM fractions from the LPS-treated mice at diverse durations post-LPS administration. Our data indicated that the kinetics of IP3R-2 expression did not alter in the MAM fractions following LPS administration (Figure 4(E) and (F)).

Altogether, we found that IP3R-1 protein expression significantly increased in the MAM fractions of the lung lysates in the ALI model.

Knockdown of IP3R-1 inhibits the MAM formation and restores mitochondrial function in a cell culture model

To determine the maximal inhibitory concentration of LPS that inhibited cell growth, we treated cultured MLE-12 cells with different doses of LPS at 5–40 μg/mL for 24 h and found that maximum inhibition of cell growth was observed at 40 μg/mL of LPS concentration (Supplementary Figure 3-A). We determined the expression kinetics of IP3R-1 following LPS treatments in cultured MLE-12 cells. We found that expression of IP3R-1 increased gradually with increasing concentrations of LPS added to the culture (Supplementary Figure 3). The morphological changes in subcellular organelles of MLE-12 cells after LPS treatment were consistent with those observed from *in vivo* ALI model (Supplementary Figure 4).

To verify the role of IP3R-1 in endotoxin attacking cell model, we utilized specific siRNA to selectively knockdown IP3R-1 expression within MLE-12 cells. The efficiency of siRNA knockdown on IP3R-1 expression was determined through quantitative reverse transcription–polymerase chain reaction (qRT-PCR) and Western-blotting analysis. The IP3R-1 mRNA expression decreased by more than 70%, while its protein level decreased by 39.9% within MLE-12 cell line (Supplementary Figure 5).

This work also investigated how IP3R-1 silencing affected MLE-12 cells after treatment with LPS in the context of MAM formation and mitochondrial RCR. Compared to negative control siRNA (NC-siRNA), we found that knockdown of IP3R-1 significantly increased the total number of mitochondria per field, decreased the relative cross-sectional area of mitochondria per field, and decreased mitochondrial membrane–adjacent ER interaction percentage when MLE-12 cells were subjected to LPS (Figure 5(A to (D))). Reduction in IP3R-1 expression level in MLE-12 cells also resulted in improved mitochondrial RCR by raising the ST3 respiratory rate while lowering the ST4 respiratory rate (Figure 6).

Furthermore, we evaluated mitochondrial Ca^{2+} uptake, mitochondrial ROS, and mitochondrial membrane potential by flow cytometry with specific probes. Based on our observations, LPS administration in MLE-12 cells increased mitochondria-to-ER transport of Ca^{2+} via MAM, thereby increasing the mitochondrial Ca^{2+} levels, which subsequently increased the production of the ROS and impaired mitochondrial function, as observed by decreased mitochondrial RCR and disrupted mitochondrial membrane potential

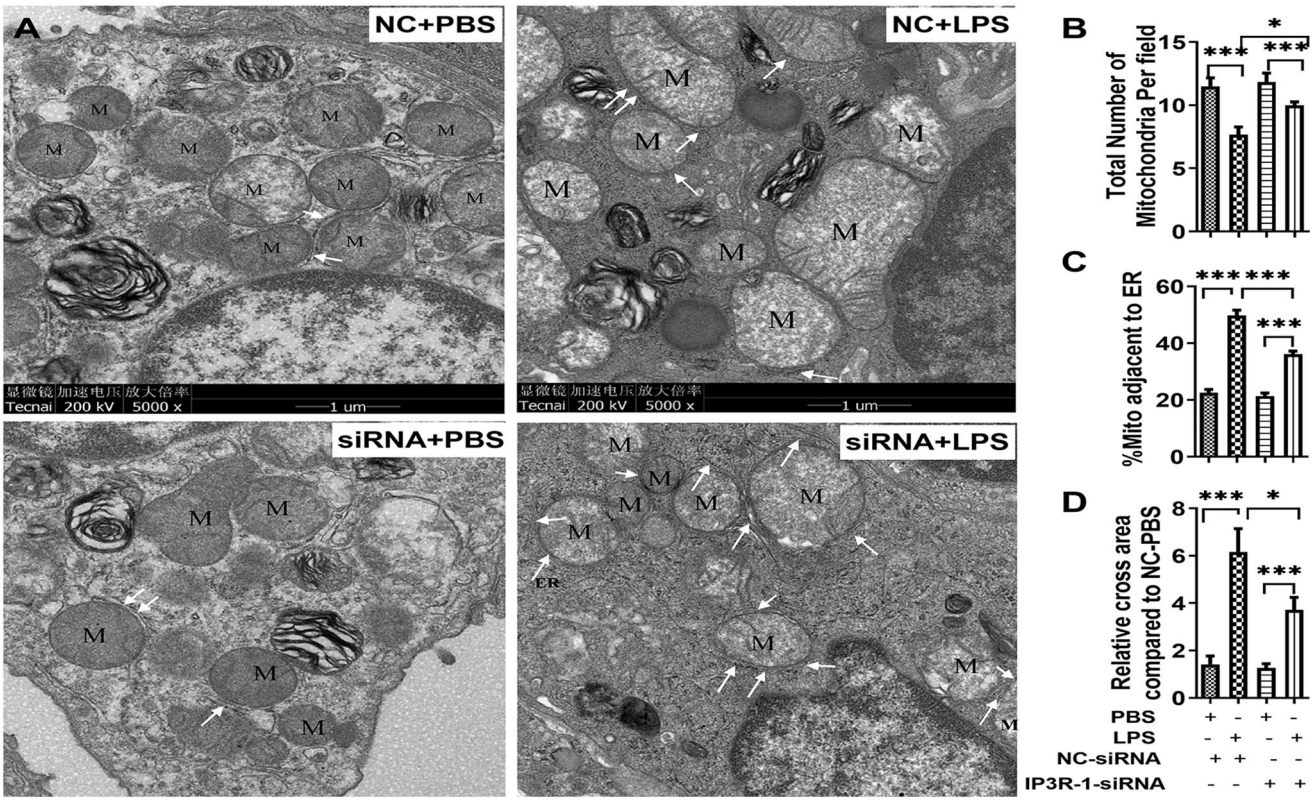

Figure 5. Specific knockdown of IP3R-1 inhibited the ER and mitochondria interaction in MLE-12 cells challenged with LPS. (A) Representative TEMs of control MLE-12 (NC-siRNA) and knockdown MLE-12 (IP3R-1 siRNA) cells following either endotoxin or PBS treatments. Scale bar: 1 μm. White arrow indicates endoplasmic reticulum interacted with mitochondria. (B) to (D) The total number of mitochondria per field (B), the cross-sectional area of mitochondria per field (C), and the ratio between the percent of mitochondria connected to ER to the total mitochondrial perimeter (D). M: mitochondria. All bars are mean ± SEM. $n = 6$; $^{*}P < 0.05$; $^{***}P < 0.001$; one-way ANOVA.

(Figure 7). Silencing IP3R-1 in MLE-12 cells partially inhibited calcium influx to mitochondria following treatment with LPS (MFI decreased from 1058 to 622).

Colocalization of VDAC-1 and IP3R-1 at the MAM was observed by immunofluorescence (Figure 8). A significant colocalization of VDAC-1 and IP3R-1 was observed in control MLE-12 cells regardless of LPS treatment (Figure 8). Low fluorescence intensity of IP3R-1 was observed in knockdown cells, indicating the efficacy of siRNA-mediated knockdown of IPR3-1 in MLE-12 cells. In IP3R-1 siRNA knockdown cells, the fluorescence intensity of IP3R-1 was much less compared to VDAC-1 regardless of LPS treatment, resulting in decreased colocalization of VDAC-1 and IP3R-1 (Figure 8). However, following LPS treatment, the fluorescence intensity of IP3R-1 protein increased in both control cells and IP3R-1 knockdown cells resulting in increased colocalization of VDAC-1 and IP3R-1. Quantification of the colocalization of VDAC-1 and IP3R-1 was performed by calculating Mander's colocalization coefficient (Figure 9(A) and (B)). Regardless of LPS treatment, the colocalization coefficient decreased in IP3R-1 knockdown cells in comparison with controls. Following LPS administration, the colocalization coefficient increased in both control cells and IP3R-1 knockdown cells.

Collectively, this loss-of-function approach supports that it is efficient to target structural and functional components of MAM for improving mitochondrial function in an ALI model.

Discussion

In this study, we demonstrated increased MAM formation, significant morphological changes in the mitochondria, and increased IP3R-1 expression in lung tissues of mice using the endotoxin-mediated ALI model. *In vitro* cell culture model, we have shown that MAM formation was reduced, and mitochondrial function was partially normalized in LPS-induced MLE-12 cells when IP3R-1 function was silenced.

Since Bernhard *et al*.[23] first discovered ER–mitochondrial contact under the electron microscope in the 1950s, various studies have displayed that more and more proteins can be detected on the MAM, which regulate the ER–mitochondrial interaction, thereby regulating various biological activities, like lipid metabolism,[24] Ca^{2+} signaling,[25] autophagy,[26] maintenance of mitochondrial structure,[27] and apoptosis.[28] It is therefore unsurprising that the MAM turn out to be highly relevant to many diseases. Earlier studies have suggested that MAM demonstrated a complex association with diabetes and cancer.[29] In recent years, emerging studies have indicated that MAM may be involved in infection and neurodegeneration disease.[30,31] However, the roles of MAM in endotoxin-induced ALI have not been fully established.

Approximately 40% of sepsis cases are prone to develop mild or severe ARDS.[32] Both mitochondrial dysfunction and ER stress have essential effects on pathogenesis of sepsis-mediated ALI and served as an indispensable signaling structure between the ER and mitochondria. We speculate

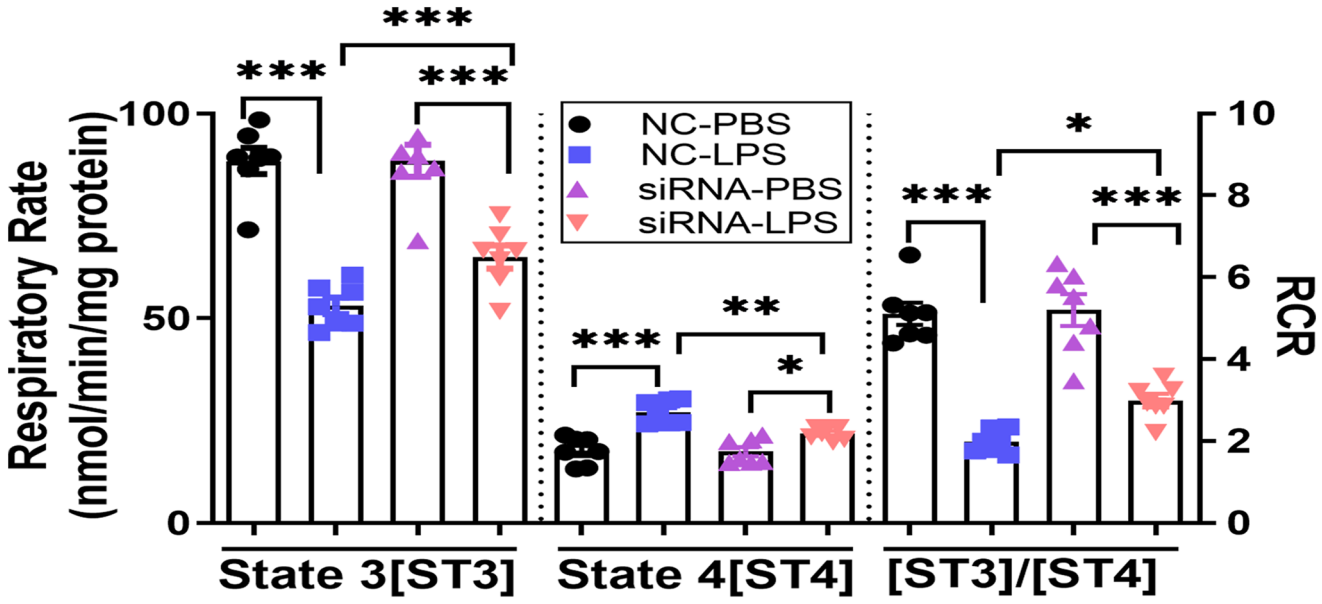

Figure 6. Oxygen consumption measurements in isolated mitochondria from MLE-12 cells under different treatments. The graph indicates the mean ± SEM. $n = 7$; *$P < 0.05$; **$P < 0.01$; ***$P < 0.001$; one-way ANOVA.

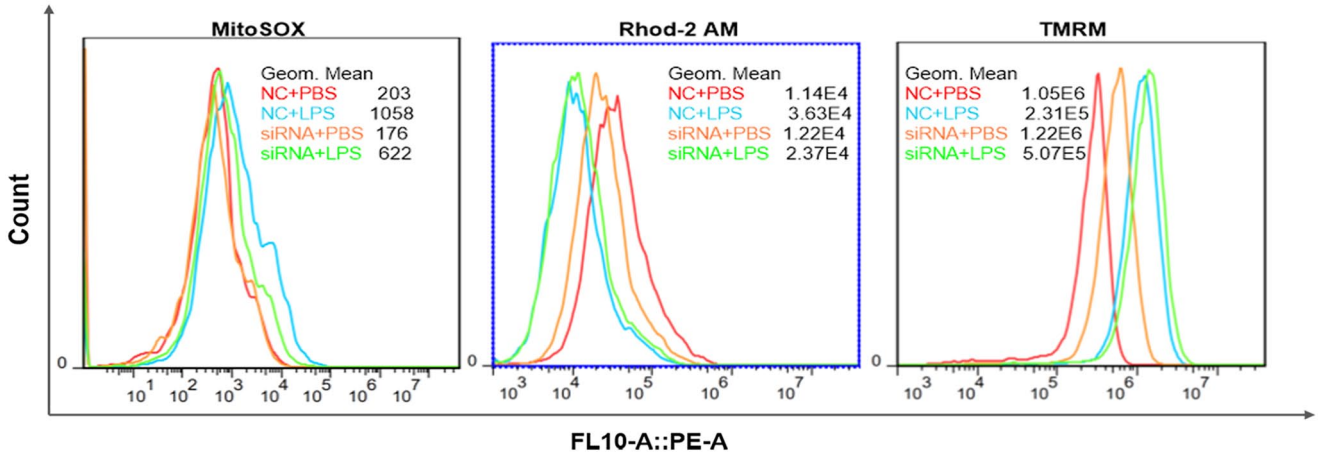

Figure 7. Mitochondrial Ca^{2+} influx, ROS, and mitochondrial membrane potential levels measured within different treated MLE-12 cells. Mitochondrial Ca^{2+} signal was determined with Rhod-2AM staining, ROS was determined with MitoSOX, mitochondrial membrane potential was analyzed with TMRM through flow cytometry. The mean fluorescence intensity (MFI) expressed as Geom. Mean is presented in each histogram overlay.

that MAM have implications for endotoxin-induced lung injury. The present work developed the endotoxin-induced ALI mouse model through LPS injection and found that increased MAM formation, altered mitochondrial morphology (including mitochondrial swelling, vacuoles formation, and crest reduction), and diminished mitochondrial oxygen consumption in the mice model of endotoxin-induced ALI. The mechanisms by which MAM promote endotoxin-induced ALI and the remedies to help reduce its formation still remain to be studied.

Mitochondria represent the powerhouses, which are important for cell metabolism, and mitochondrial dysfunction has been shown to be the cause of the initiation and exacerbation of acute lung injury.[33] Accordingly, improving mitochondrial function is of great importance for the treatment of lung injury. Mitochondria show high dynamics, with constant fusion, division, and migration along cytoskeleton for forming a mitochondria network, and studies involving mitochondrial dynamics and MAM in recent years mainly focus on mechanism of mitochondrial fission and fusion.[34] As a necessary component for mitochondrial dehydrogenase function during cellular respiration and Kreb's cycle, Ca^{2+} exerts a critical effect on regulating mitochondrial function.[35] Specific proteins have been identified in MAM for maintaining optimum distance between organelles and co-ordinate Ca^{2+} transporters or channels between mitochondria and ER, including Sig-1R, IP3R, mitofusin, and phosphofurin acidic cluster sorting protein-2 (PACS-2).[36–38] In this study, MAM-related protein levels were analyzed within mice lung lysates after LPS induction, as a result, IP3R-1, which is responsible for Ca^{2+} transport, was significantly upregulated, suggesting the enhanced ER-to-mitochondria transport of Ca^{2+}. In addition, mitochondrial fusion protein Mfn-2 expression decreased, which was consistent with our

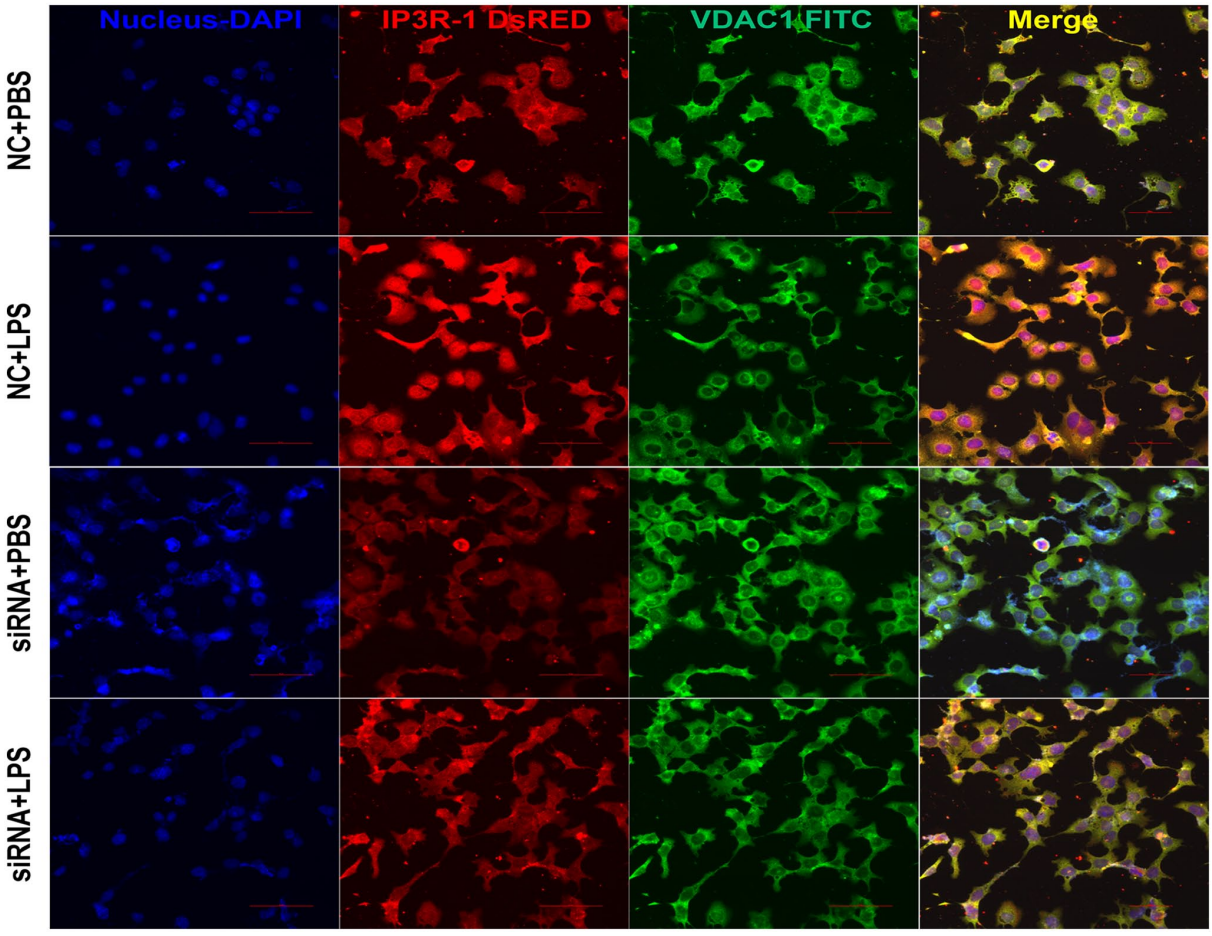

Figure 8. Visualization of the VDAC-1/IP3R-1 complex by immunofluorescence. VDAC-1 was stained with DsRED (red), IPR3-1 was stained using FITC (green), whereas nucleus was stained using DAPI (blue). The yellow color on the merged images illustrates colocalization between VDAC-1 and IPR3-1. Scale bar = 50 µm.

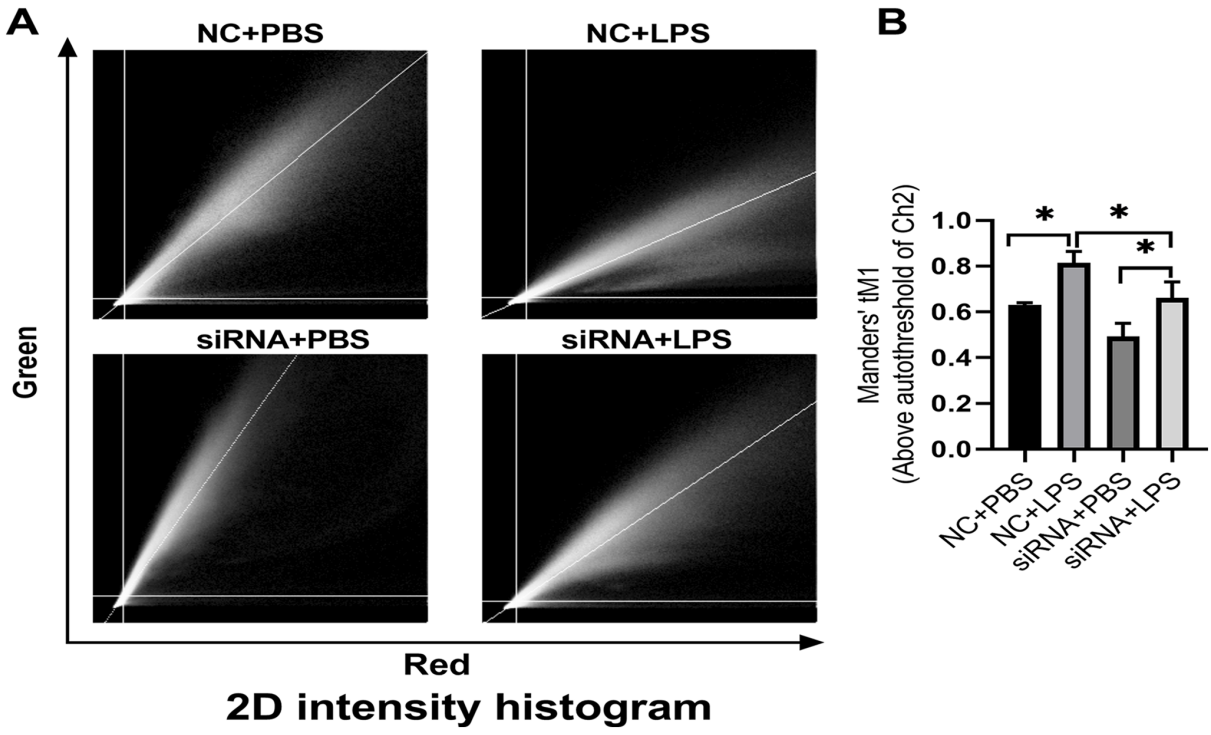

Figure 9. Knockdown of IP3R-1 decreased the colocalization coefficient in MLE-12 cells challenged with LPS. (A) and (B) Quantification of the colocalization of VDAC-1 and IP3R-1 was performed by calculating Mander's colocalization coefficient. The graph represents mean ± SEM; $n = 3$; $^*P < 0.05$; one-way ANOVA.

previous experimental results,[5,6] suggesting that the proportion of mitochondria in the state of division correspondingly increased. Furthermore, we collected different subcellular components in mouse lungs, including PM, CM, MAM, and ER by Percoll-based density gradient centrifugation and further found that the level of IP3R-1 increased and Mfn-2 declined within purified MAM in comparison with control group. In addition, we reported that in LPS-mediated ALI mouse lungs, several changes in mitochondrial homeostatic functions were observed, such as increased Ca^{2+} concentration, significantly decreased membrane potential, increased ROS production, reduced respiratory control rate, and extremely impaired mitochondrial function. Therefore, we hypothesized that MAM formation was elevated, and IP3R-1 expression was significantly upregulated among ALI mice caused by LPS, which resulted in calcium overload in the mitochondria leading to mitochondrial dysfunction.

To confirm the role of IP3R-1 on mitochondrial function during acute lung injury, IP3R-1 knockdown MLE-12 cells were exposed to LPS. As expected, IP3R-1 knockdown significantly reduced MAM formation compared to the control cells in response to LPS. Concomitantly, the levels of Ca^{2+} and ROS production were reduced in the mitochondria, and mitochondrial membrane potential and respiratory control rate were improved significantly in IP3R-1 knockdown MLE-12 cells. VDAC-1 is a MAM tether protein that is involved in Ca^{2+} accumulation in the mitochondria.[39,40] Szabadkai *et al*.[13] found that VDAC-1 bound to ligand-binding domain of IP3R-1 and facilitates mitochondrial Ca^{2+} uptake. In this study, we used immunofluorescence for the visualization of the VDAC-1/IP3R-1 complex and found that VDAC-1-to-IP3R-1 connection was enhanced during the LPS administration which facilitated ER-to-mitochondrial transport of Ca^{2+}, then causing mitochondrial impairment; however, knocking down IP3R-1 could hamper the connection when the MLE-12 cells were exposed to LPS. To sum up, these results suggested that downregulation of IP3R-1 expression dramatically reduced mitochondrial calcium overload and alleviated mitochondrial dysfunction.

Certain limitations should be noted in this work. First, this work analyzed effect of IP3R-1 on MAM formation and mitochondrial function, but the upstream as well as downstream regulators for IP3R-1 signaling pathway should be further elucidated in ALI model. Second, in this study, the siRNA method was used to silence IP3R-1 function only in the endotoxin-induced cell culture model. Studies on conditional IP3R-1 knockout mice may provide more insights into the mitochondrial function in the endotoxin-induced ALI model. Expression analysis of IP3R-1 in the MAM of clinical patients with sepsis constitutes our next research direction. Third, Desouza *et al*.[41] ascertained that IP3R was a key locus for the regulation of proapoptotic and antiapoptotic factors. Therefore, the influence of IP3R-1 on apoptosis via the mitochondrial pathway in ALI remains to be explored. Finally, we notice that the expression levels of Mfn-2 in the MAM are considerably downregulated in the ALI model, but the exact role and mechanism by which Mfn-2 promotes the formation of MAM remain to be seen, and further research is required.

In conclusion, as demonstrated by this study, IP3R-1 contributes to MAM formation and mitochondrial oxidative stress during endotoxin-induced ALI primarily by means of mitochondrial dysfunction caused by Ca^{2+} overload. This being the case, it is conceivable that targeted inhibition of IP3R-1 function may become an effective strategy to treat lung injury in sepsis patients.

AUTHORS' CONTRIBUTIONS

Our authors made significant contributions to this work and manuscript preparation. SD, YW, and JY conceived the study. YZ analyzed the data with assistance from ShaoL, QZ, ShasL, and YG. SD and YW wrote the manuscript. XL, KS, LilW, LinW, JS, and LG reviewed the manuscript. JY guided the proposed model. Our authors agreed to the final manuscript for submission.

DECLARATION OF CONFLICTING INTERESTS

The author(s) declared no potential conflicts of interest with respect to the research, authorship, and/or publication of this article.

ETHICAL APPROVAL

This work gained approval from the Animal Care and Use Committee of the Tianjin Nankai Hospital (approval no. NKYY-DWLL-2019-027, Tianjin, China) and was carried out following the legislation on laboratory animals.

FUNDING

The author(s) disclosed receipt of the following financial support for the research, authorship, and/or publication of this article: This study was funded by the National Natural Science Foundation of China (82002069, 82074153) and the Natural Science Foundation of Tianjin (20JCYBJC00540, 21JCZDJC01120, TJSQNYXXR-D2-154).

ORCID IDS

Ya Wu https://orcid.org/0000-0002-8131-994X

Jianbo Yu https://orcid.org/0000-0003-0530-6749

SUPPLEMENTAL MATERIAL

Supplemental material for this article is available online.

REFERENCES

1. Singer M, Deutschman CS, Seymour CW, Shankar-Hari M, Annane D, Bauer M, Bellomo R, Bernard GR, Chiche JD, Coopersmith CM, Hotchkiss RS, Levy MM, Marshall JC, Martin GS, Opal SM, Rubenfeld GD, van der Poll T, Vincent JL, Angus DC, et al. The third international consensus definitions for sepsis and septic shock (Sepsis-3). *JAMA* 2016;**315**:801–10
2. Cuthbertson BH, Elders A, Hall S, Taylor J, MacLennan G, Mackirdy F, Mackenzie SJ; Scottish Critical Care Trials Group; Scottish Intensive Care Society Audit Group. Mortality and quality of life in the five years after severe sepsis. *Crit Care* 2013;**17**:R70
3. Liang L, Moore B, Soni A. National inpatient hospital costs: the most expensive conditions by payer. 2017, https://www.ncbi.nlm.nih.gov/books/NBK561141/
4. Millar FR, Summers C, Griffiths MJ, Toshner MR, Proudfoot AG. The pulmonary endothelium in acute respiratory distress syndrome: insights and therapeutic opportunities. *Thorax* 2016;**71**:462–73
5. ARDS Definition Task Force; Ranieri VM, Rubenfeld GD, Thompson BT, Ferguson ND, Caldwell E, Fan E, Camporota L, Slutsky AS. Acute respiratory distress syndrome: the Berlin Definition. *JAMA* 2012;**307**:2526–33

6. Shi J, Yu J, Zhang Y, Wu L, Dong S, Wu L, Wu L, Du S, Zhang Y, Ma D. PI3K/Akt pathway-mediated HO-1 induction regulates mitochondrial quality control and attenuates endotoxin-induced acute lung injury. *Lab Invest* 2019;**99**:1795–809
7. Kim HJ, Jeong JS, Kim SR, Park SY, Chae HJ, Lee YC. Inhibition of endoplasmic reticulum stress alleviates lipopolysaccharide-induced lung inflammation through modulation of NF-kappaB/HIF-1alpha signaling pathway. *Sci Rep* 2013;**3**:1142
8. Almannai M, El-Hattab AW, Ali M, Soler-Alfonso C, Scaglia F. Clinical trials in mitochondrial disorders, an update. *Mol Genet Metab* 2020;**131**:1–13
9. Csordás G, Renken C, Várnai P, Walter L, Weaver D, Buttle KF, Balla T, Mannella CA, Hajnóczky G. Structural and functional features and significance of the physical linkage between ER and mitochondria. *J Cell Biol* 2006;**174**:915–21
10. Murley A, Lackner LL, Osman C, West M, Voeltz GK, Walter P, Nunnari J. ER-associated mitochondrial division links the distribution of mitochondria and mitochondrial DNA in yeast. *Elife* 2013;**2**:e422
11. Rizzuto R, De Stefani D, Raffaello A, Mammucari C. Mitochondria as sensors and regulators of calcium signalling. *Nat Rev Mol Cell Biol* 2012;**13**:566–78
12. Patergnani S, Danese A, Bouhamida E, Aguiari G, Previati M, Pinton P, Giorgi C. Various aspects of calcium signaling in the regulation of apoptosis, autophagy, cell proliferation, and cancer. *Int J Mol Sci* 2020;**21**:8323
13. Szabadkai G, Bianchi K, Várnai P, De Stefani D, Wieckowski MR, Cavagna D, Nagy AI, Balla T, Rizzuto R. Chaperone-mediated coupling of endoplasmic reticulum and mitochondrial Ca2+ channels. *J Cell Biol* 2006;**175**:901–11
14. Rizzuto R, Brini M, Murgia M, Pozzan T. Microdomains with high Ca2+ close to IP3-sensitive channels that are sensed by neighboring mitochondria. *Science* 1993;**262**:744–7
15. Kirichok Y, Krapivinsky G, Clapham DE. The mitochondrial calcium uniporter is a highly selective ion channel. *Nature* 2004;**427**:360–4
16. Arruda AP, Pers BM, Parlakgül G, Güney E, Inouye K, Hotamisligil GS. Chronic enrichment of hepatic endoplasmic reticulum-mitochondria contact leads to mitochondrial dysfunction in obesity. *Nat Med* 2014;**20**:1427–35
17. Rowland AA, Voeltz GK. Endoplasmic reticulum-mitochondria contacts: function of the junction. *Nat Rev Mol Cell Biol* 2012;**13**:607–25
18. Area-Gomez E, Del Carmen Lara Castillo M, Tambini MD, Guardia-Laguarta C, de Groof AJ, Madra M, Ikenouchi J, Umeda M, Bird TD, Sturley SL, Schon EA. Upregulated function of mitochondria-associated ER membranes in Alzheimer disease. *Embo J* 2012;**31**:4106–23
19. Tubbs E, Theurey P, Vial G, Bendridi N, Bravard A, Chauvin MA, Ji-Cao J, Zoulim F, Bartosch B, Ovize M, Vidal H, Rieusset J. Mitochondria-associated endoplasmic reticulum membrane (MAM) integrity is required for insulin signaling and is implicated in hepatic insulin resistance. *Diabetes* 2014;**63**:3279–94
20. Wieckowski MR, Giorgi C, Lebiedzinska M, Duszynski J, Pinton P. Isolation of mitochondria-associated membranes and mitochondria from animal tissues and cells. *Nat Protoc* 2009;**4**:1582–90
21. Matute-Bello G, Downey G, Moore BB, Groshong SD, Matthay MA, Slutsky AS, Kuebler WM; Acute Lung Injury in Animals Study Group. An official American thoracic society workshop report: features and measurements of experimental acute lung injury in animals. *Am J Respir Cell Mol Biol* 2011;**44**:725–38
22. Dong SA, Zhang Y, Yu JB, Li XY, Gong LR, Shi J, Kang YY. Carbon monoxide attenuates lipopolysaccharide-induced lung injury by mitofusin proteins via p38 MAPK pathway. *J Surg Res* 2018;**228**:201–10
23. Bernhard W, Haguenau F, Gautier A, Oberling C. [Submicroscopical structure of cytoplasmic basophils in the liver, pancreas and salivary gland; study of ultrafine slices by electron microscope]. *Z Zellforsch Mikrosk Anat* 1952;**37**:281–300
24. Vance JE. Phospholipid synthesis and transport in mammalian cells. *Traffic* 2105;**16**:1–18
25. Duchen MR. Ca(2+)-dependent changes in the mitochondrial energetics in single dissociated mouse sensory neurons. *Biochem J* 1992;**283**:41–50
26. Hailey DW, Rambold AS, Satpute-Krishnan P, Mitra K, Sougrat R, Kim PK, Lippincott-Schwartz J. Mitochondria supply membranes for autophagosome biogenesis during starvation. *Cell* 2010;**141**:656–67
27. Galmes R, Houcine A, van Vliet AR, Agostinis P, Jackson CL, Giordano F. ORP5/ORP8 localize to endoplasmic reticulum-mitochondria contacts and are involved in mitochondrial function. *EMBO Rep* 2016;**17**:800–10
28. Mochida K, Oikawa Y, Kimura Y, Kirisako H, Hirano H, Ohsumi Y, Nakatogawa H. Receptor-mediated selective autophagy degrades the endoplasmic reticulum and the nucleus. *Nature* 2015;**522**:359–62
29. Bononi A, Bonora M, Marchi S, Missiroli S, Poletti F, Giorgi C, Pandolfi PP, Pinton P. Identification of PTEN at the ER and MAMs and its regulation of Ca(2+) signaling and apoptosis in a protein phosphatase-dependent manner. *Cell Death Differ* 2013;**20**:1631–43
30. Horner SM, Liu HM, Park HS, Briley J, Gale MJ. Mitochondrial-associated endoplasmic reticulum membranes (MAM) form innate immune synapses and are targeted by hepatitis C virus. *Proc Natl Acad Sci U S A* 2011;**108**:14590–5
31. Paillusson S, Stoica R, Gomez-Suaga P, Lau DHW, Mueller S, Miller T, Miller CCJ. There's something wrong with my MAM; the ER-mitochondria axis and neurodegenerative diseases. *Trends Neurosci* 2016;**39**:146–57
32. Sessler CN, Bloomfield GL, Fowler AA 3rd. Current concepts of sepsis and acute lung injury. *Clin Chest Med* 1996;**17**:213–35
33. Howell MD, Davis AM. Management of sepsis and septic shock. *JAMA* 2017;**317**:847–8
34. Friedman JR, Lackner LL, West M, DiBenedetto JR, Nunnari J, Voeltz GK. ER tubules mark sites of mitochondrial division. *Science* 2011;**334**:358–62
35. Cárdenas C, Miller RA, Smith I, Bui T, Molgó J, Müller M, Vais H, Cheung KH, Yang J, Parker I, Thompson CB, Birnbaum MJ, Hallows KR, Foskett JK. Essential regulation of cell bioenergetics by constitutive InsP3 receptor Ca2+ transfer to mitochondria. *Cell* 2010;**142**:270–83
36. Thomas G, Aslan JE, Thomas L, Shinde P, Shinde U, Simmen T. Caught in the act – protein adaptation and the expanding roles of the PACS proteins in tissue homeostasis and disease. *J Cell Sci* 2017;**130**:1865–76
37. Vannuvel K, Renard P, Raes M, Arnould T. Functional and morphological impact of ER stress on mitochondria. *J Cell Physiol* 2013;**228**:1802–18
38. Hayashi T, Su TP. Sigma-1 receptor chaperones at the ER-mitochondrion interface regulate Ca(2+) signaling and cell survival. *Cell* 2007;**131**:596–610
39. Xu H, Guan N, Ren YL, Wei QJ, Tao YH, Yang GS, Liu XY, Bu DF, Zhang Y, Zhu SN. IP3R-Grp75-VDAC1-MCU calcium regulation axis antagonists protect podocytes from apoptosis and decrease proteinuria in an Adriamycin nephropathy rat model. *BMC Nephrol* 2018;**19**:140
40. Szabadkai G, Duchen MR. Mitochondria: the hub of cellular Ca2+ signaling. *Physiology* 2008;**23**:84–94
41. Desouza N, Reiken S, Ondrias K, Yang Y, Matkovich S, Marks AR. Protein kinase A and two phosphatases are components of the inositol 1,4,5-trisphosphate receptor macromolecular signaling complex. *J Biol Chem* 2002;**277**:39397–400

(Received July 25, 2023, Accepted October 2, 2023)